Journal of Alloys and Compounds 509 (2011) 1861–1865

Contents lists available at ScienceDirect

Journal of Alloys and Compounds

journal homepage: www.elsevier.com/locate/jallcom

Effect of calcination temperature on the structural and electrical properties of cobalt ferrite synthesized by combustion method

M.S. Khandekar[a], R.C. Kambale[b], J.Y. Patil[a], Y.D. Kolekar[c], S.S. Suryavanshi[a,*]

[a] Ferrite Materials Laboratory, Department of Physics, Solapur University, Solapur 413255, MS, India
[b] Composite Materials Laboratory, Department of Physics, Shivaji University, Kolhapur 416004, MS, India
[c] Department of Physics, University of Pune, Ganeshkhind, Pune 411007, MS, India

ARTICLE INFO

Article history:
Received 7 October 2009
Received in revised form 14 October 2010
Accepted 22 October 2010
Available online 30 October 2010

Keywords:
Magnetically ordered materials
Chemical synthesis
X-ray diffraction
Dielectric response
Electrical transport
Thermal analysis

ABSTRACT

In this paper, the structural and electrical properties of cobalt ferrite synthesized by combustion route with hexamine as a fuel are reported for the first time. Thermogravemetric analysis (TGA) confirm the stable phase formation of the phase above 700 °C. Structural characterizations of all the samples were carried out by X-ray diffraction (XRD) technique. It reveals an increase in the particle size with the calcination temperature (i.e. 700, 800 and 900 °C). Infrared (IR) spectroscopy confirms the presence of tetrahedral and octahedral group complexes within the spinel lattice. DC resistivity as function of temperature indicates that all the samples obey the semiconducting behavior and it decreases with calcination temperature. The variation of dielectric constant (ε_r) and ac conductivity (σ_{ac}), for all the samples have been studied as a function of applied frequency in the range from 20 Hz to 1 MHz. The dielectric constant increases with the calcination temperature and all the samples exhibit usual dielectric dispersion which is due to the Maxwell–Wagner-type interfacial polarization. The ac conductivity measurement suggests that the conduction is due to small polaron hopping.

1. Introduction

Ferrites have diverse practical applications such as magnetic materials [1,2], refractory materials [3], in medical diagnostics [4,5], and as catalysts [6]. $CoFe_2O_4$ has been a topic of intensive research in recent years. It is one of the good candidate for high-density magneto-optic recording applications due to its high coercivity, high magnetocrystalline anisotropy and moderate saturation magnetization [7,8]. It has been reported that, the properties of ferrite nano particles are strongly influenced by its composition and microstructure which are very much sensitive to the method of preparation. Various methods have been developed to synthesize nanocrystalline $CoFe_2O_4$, namely: co-precipitation [9], mechano-chemical [10], combustion [11], micro-emulsion [12], redox process [13], hydrothermal [14], sol–gel [15], forced hydrolysis [16]. Among these, combustion method seems to be one of the facile and one step methods, since it allows the preparation of nanocrystalline $CoFe_2O_4$ with an equiaxial shape and narrow size distribution. The fuels so far employed in the combustion synthesis are urea, glycine, oxalyldihydrazide (ODH), carbohydrazide (CH), tetraformaltrisazine (TFTA), N,N-diformylhydrazine (DFH), etc. By employing these fuels, a large number of oxides have been synthesized [17]. Except for urea and glycine, most of the other fuels used in the combustion synthesis are hydrazine derivatives prepared using hydrazine hydrate, which is carcinogenic. Therefore, it is considered worthwhile to search for alternative fuels that are inexpensive, readily available, and can be used for the preparation of a large variety of oxides. Hexamethylenetetramine (HMT), $(CH_2)_6N_4$, also known as hexamine, is a versatile reagent in organic synthesis [18].

However, ferrites are commonly produced by a ceramic process involving high-temperature solid-state reactions between the constituent oxides or carbonates. The size of the particles obtained by this process is rather large and non-uniform. These non-uniform particles, on compacting, result in the formation of voids or low density. In order to overcome these difficulties arising out of the ceramic route, wet chemical methods like co-precipitation, hydrothermal processing, combustion, etc. have been considered for production of homogeneous, fine and reproducible ferrites [19]. Koops [20] subjected a series of Ni–Zn ferrites all of the same composition but to various sintering conditions and explained the variation in resistivity and dielectric constant to the presence of Fe^{2+} concentration developed during the sintering. In the present paper, we report the synthesis of $CoFe_2O_4$ using combustion route at a lower processing temperature and also report the effect of calcination temperature on its structural and electrical properties.

* Corresponding author. Tel.: +91 217 2744771; fax: +91 217 2744770.
E-mail address: sssuryavanshi@rediffmail.com (S.S. Suryavanshi).

0925-8388/$ – see front matter © 2010 Elsevier B.V. All rights reserved.
doi:10.1016/j.jallcom.2010.10.073

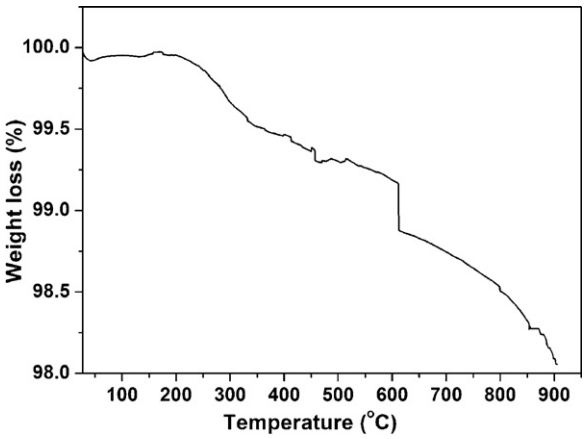

Fig. 1. Typical TGA curve for as synthesized powder of $CoFe_2O_4$ ferrite.

2. Experimental details

2.1. Synthesis

Cobalt ferrite was synthesized by the chemical autocombustion route, in which the stoichiometric amount of the corresponding metal nitrates acts as an oxidizing agent and the fuel hexamine as a reducing agent for the combustion reaction. The stoichiometry of the redox mixture for combustion is calculated based on the total oxidizing and reducing valencies of oxidizer (O) and fuel (F) [21], which serves as a numerical coefficient so that the equivalence ratio, i.e. the (O/F), becomes unity and the heat released is at its maximum [22,23]. Hence, in order to release the maximum energy for the combustion reaction, the stoichiometric composition of the redox mixture requires $-40+36n=0$ or $n=1.11$ mol of hexamine. Therefore, the molar ratio, i.e. φ_e (O/F), of the oxidizing metal nitrate to the reducing fuel (hexamine) is 40/36 = 1.11 (i.e. the proportion of M^{2+}:Fe^{3+}:fuel should be 1:2:1.11).

Thus, a mixture of $Co(NO_3)_2{\cdot}6H_2O$and $Fe(NO_3)_3{\cdot}9H_2O$ in an appropriate molar proportion was taken in a 300 cm^3 capacity Pyrex dish and was melted by heating on a magnetic stirrer at 80 °C for 15 min. Further, hexamine was added to the melt and the slurry formed was further heated up to ~500 °C on electric heater for combustion. It is observed that after evaporation of the water content, the mixture frothed and ignited to combust (Smouldering) with an evaporation of large amount of gases, giving a voluminous and foamy $CoFe_2O_4$ as a product.

The formation of $CoFe_2O_4$ by combustion reaction using hexamine is shown below:

$$CO(NO_3)_2 \cdot 6H_2O + 2Fe(NO_3)_3 \cdot 9H_2O + 1.11C_6H_{12}N_4 \xrightarrow{\Delta} COFe_2O_4 + 6.22N_2 \uparrow + 6.66CO_2 \uparrow + 30.66H_2O \uparrow$$

The resulting powder was further characterized by Thermogravemetric analysis (TGA) by means of SDT 2960 simultaneous DSC-TGA TA instruments USA at a heating rate of 10 °C min^{-1} in an air stream. For the phase identification, the samples were characterized by the powder x-ray diffraction (XRD) technique (Cu Kα radiation, model Bruker D8 Advance). For all electrical measurements, the disk shaped pellets (1–2 mm in thickness and 15 mm in diameter) were coated with silver paint on both sides and heated in a furnace at 200 °C for 1–2 h to get good ohmic contacts with the electrodes during measurements. The DC resistivity measurement as a function of temperature (room temperature to 500 °C) was carried out by two-probe method, where Keithley electrometer (model 6514) was used to record the resistance of the sample. The dielectric constant (ε'), dielectric loss ($\tan\delta$) and ac conductivity (σ_{ac}) were measured at room temperature as a function of applied frequency in the range 100 Hz to 1 MHz using an LCR precision meter (HP 4284A).

3. Results and discussion

3.1. Thermogravemetric analysis (TGA)

Fig. 1 shows the typical TGA curve for as synthesized powder of $CoFe_2O_4$ sample. There is a total weight loss of 2% is observed within the temperature range of 180–600 and 600–900 °C. During combustion process high ignition temperature is present which forms the oxides at this instant only, therefore the sample show low weight loss with respect to temperature. The first step of weight loss is 1% of the total weight, corresponding to the volatilization of the organic solvent and water of crystallization. In the second step of weight loss, the weight loss is 1% ascribed to the decomposition of nitrate and complex ferrite precursors into oxides. For temperatures from 600 to 900 °C there is approximately 1% weight loss process, which shows the stable phase formation of the cobalt ferrite particles above 600 °C. Thus, the sample of $CoFe_2O_4$ was further calcined at 700 °C (Co 7), 800 °C (Co 8) and 900 °C (Co 9) for 2 h at a heating rate of 2 °C min^{-1} in an air stream and characterized by various measurement techniques.

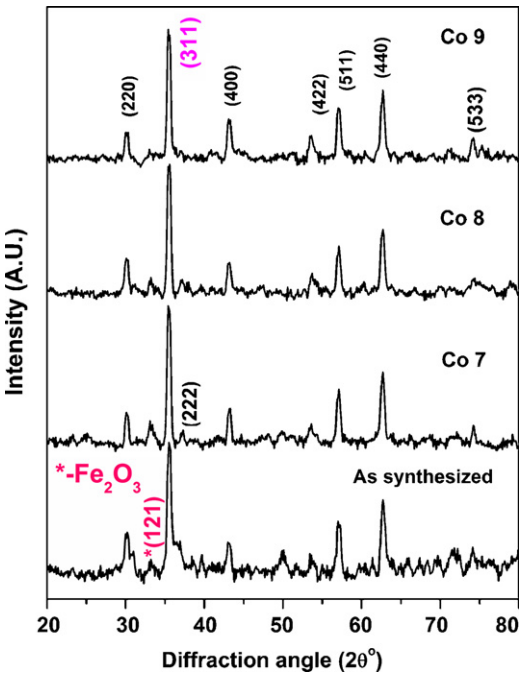

Fig. 2. The room temperature X-ray diffractograms for $CoFe_2O_4$ ferrite.

3.2. Phase analysis

Fig. 2 shows the X-ray diffraction (XRD) patterns for as synthesized and for calcined samples of $CoFe_2O_4$ system. The as synthesized sample shows the presence of hematite phase in the sample. As the calcination temperature increases the reflection corresponding to Hematite phases vanishes. All the samples show characteristic reflections of ferrite material with the most intense (3 1 1) reflection which confirms the formation of a cubic spinel structure. The results obtained by X-ray diffraction patterns were indexed using the standard JCPDS card no. 22-1086. The lattice constant for as prepared samples is found to be ~8.38 Å.

The particle size of the synthesized $CoFe_2O_4$ samples were estimated from X-ray peak broadening of the (3 1 1) peak using Scherrer formula:

$$D = \frac{0.9\lambda}{\beta \cos\theta} \quad (1)$$

where D is the particle size, λ is the wavelength of Cu Kα, β is the full width at half maxima (FWHM) of the (3 1 1) diffraction peaks and θ is the Bragg's angle. Fig. 3 shows the variation of particle size with calcination temperature, which reveals that the particle size of $CoFe_2O_4$ is sensitive to the calcination temperature.

3.3. IR spectroscopy

Fig. 4 shows the FTIR absorption bands of $CoFe_2O_4$ system calcined at 700, 800 and 900 °C were recorded at room temperature in the wavenumber range 400–2000 cm^{-1} wavenumber range. According to Waldron [24], ferrites can be considered continu-

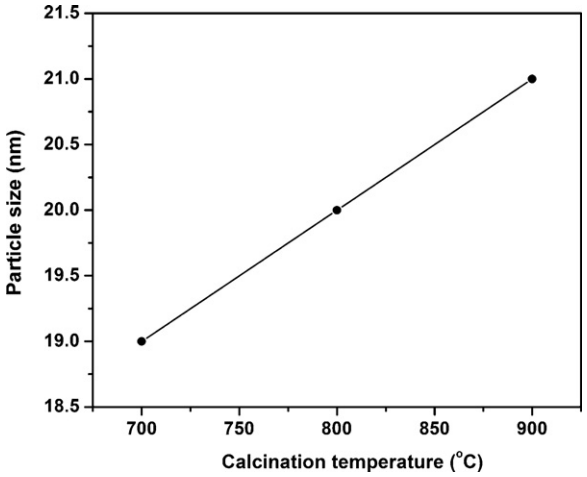

Fig. 3. Variation of the particle sizes with calcination temperature.

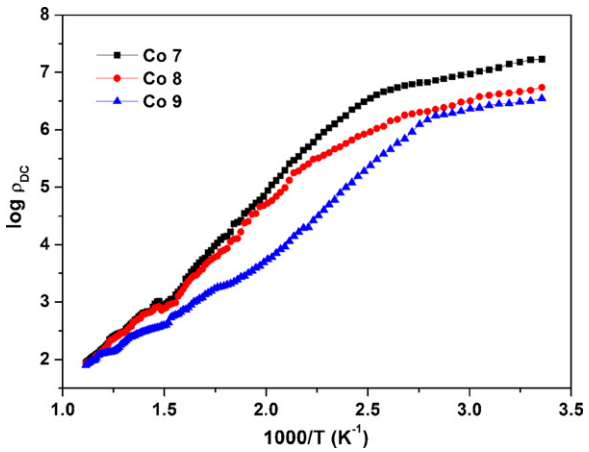

Fig. 5. Variation of DC resistivity for $CoFe_2O_4$ as a function of temperature.

ously bonded crystals, that is the atoms are bonded to all nearest neighbours by equivalent forces (ionic, covalent or van der Waals). In ferrites the metal ions are situated at two different sublattices designated tetrahedral (A-site) and octahedral (B-site) according to the geometrical configuration of the oxygen nearest neighbours. According to Waldron [24] the band ν_1 is attributed to the stretching vibration of Fe^{3+}–O^{2-} in tetrahedral complexes and ν_2 is assigned to that of bending vibrations in octahedral complexes. The position and intensities of ν_1 and ν_2 vary slightly due to the difference in the Fe^{3+}–O^{2-} distances for the tetrahedral and octahedral sites. In the present case the bands ν_1 appears near at 773, 748 and 744 cm^{-1} for Co 7, Co 8 and Co 9, respectively, which shows the shifting of ν_1 towards lower frequency with increase in calcination temperature. The second absorption band ν_2 appears near at 496, 470 and 469 cm^{-1} for Co 7, Co 8 and Co 9, respectively, which also shifts towards lower frequency with increase in calcination temperature. The differences in frequencies between ν_1 and ν_2 are due to changes in band length (Fe^{3+}–O^{2-}) at octahedral and tetrahedral sites [24]. The broad spectra for all the samples are observed. Such broadening is commonly observed for inverse spinel ferrites (MFe_2O_4). The broadening may be due to the statistical distribution of Fe at A and B site.

3.4. Electrical properties

3.4.1. DC resistivity

Variation of DC resistivity for $CoFe_2O_4$ as a function of temperature is shown in Fig. 5. The resistivity is observed to decrease exponentially with increase in temperature, which corresponds to the semiconducting behavior of the materials. The decrease in resistivity with increase in temperature may be due to the increase in drift mobility of the charge carriers [25]. Further the conduction in ferrites is attributed to the hopping of electrons from Fe^{3+} to Fe^{2+} ions [26]. The number of such ion pairs depends upon the calcination conditions and the amount of reduction of Fe^{3+} to Fe^{2+} at elevated temperatures. The resistivity of ferrite is controlled by the Fe^{2+} concentration on the B-site. In the present case the resistivity is found to be decrease with calcination temperature. Such kind of variation in DC resistivity can be explained on the basis of microstructural changes occurred in the samples due to different calcination conditions. As per above discussion the values of particle sizes are found to increase with increase in calcination temperature and thus which causes the decrease in resistivity. Verwey and De Boer [26,27] have established that in oxides, containing ions of a given element present in more than one valence state, conduction takes place through hopping of electrons between trivalent and divalent iron ions within the octahedral positions without causing a change in the energy state of a crystal as a result of the transitions. Obviously, the more the divalent iron content the higher the conduction and consequently a decrease in the resistivity is observed. The decrease in DC resistivity with the increase of sintering temperature has been attributed to the presence of increase in divalent iron content. The increasing values of particle size with increasing calcination temperature (Fig. 3) also contribute to lower the resistivity which may be due to the decrease in the activation energies from 0.25 eV to 0.20 eV [28].

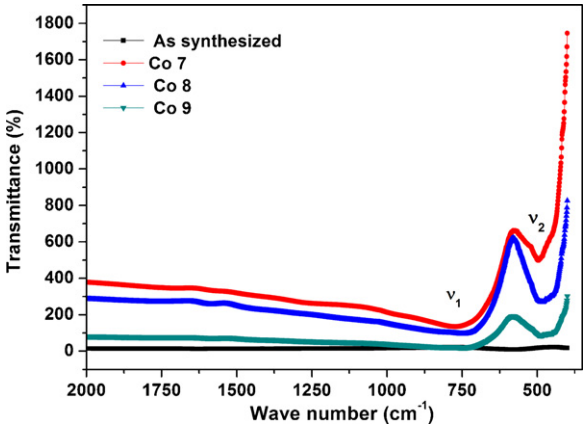

Fig. 4. FTIR absorption bands of $CoFe_2O_4$ system.

The temperature dependence of resistivity is given by the Arrhenius equation viz.

$$\rho = \rho_0 \exp\left(\frac{E_a}{k_B T}\right) \quad (2)$$

where ρ_0 is the pre-exponential factor with the dimensions of Ω cm, k_B is the Boltzmann constant, E_a is the activation energy and T is the absolute temperature.

3.4.2. Dielectric constant and ac conductivity

The dielectric constant (ε') of the sample was calculated using the relation [29]:

$$\varepsilon_r = \frac{Cd}{\varepsilon_0 A} \quad (3)$$

where C is the measured value of capacitance of the sample, d is the thickness, A is the surface area, and ε_0 is the dielectric permittivity of air (8.854×10^{-14} F/cm). The ac conductivity was measured

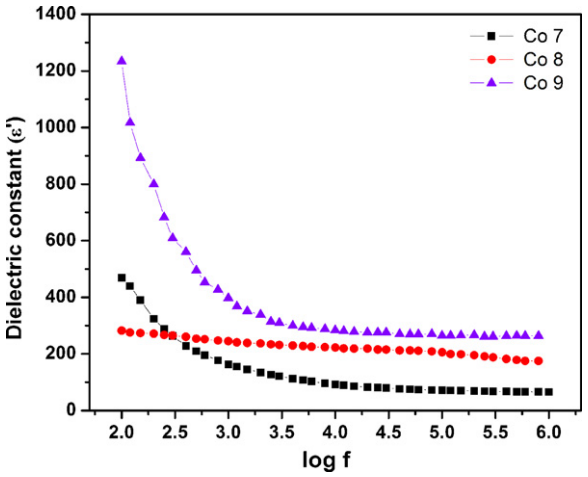

Fig. 6. Variation of dielectric constant (ε') with frequency f for $CoFe_2O_4$ system.

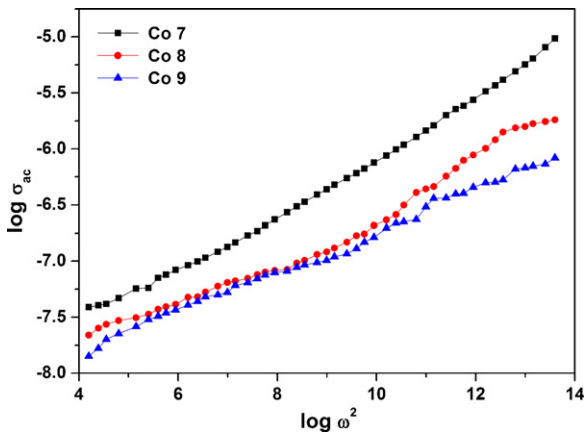

Fig. 7. Variation of AC conductivity as a function of frequency for $CoFe_2O_4$ system.

by measuring the ac resistance (R_{ac}) of the sample with respect to frequency (100 Hz to 1 MHz).

3.4.2.1. Dielectric constant. Fig. 6 shows the variation of relative dielectric constant (ε') with frequency f. It has been found that the relative dielectric constant decreases steeply at lower frequencies and remains constant at higher frequencies, indicating the usual dielectric dispersion. This may be attributed to the polarization due to changes in valence states of cations and space charge polarization. At higher frequencies the dielectric constant remains independent of frequency due to the inability of electric dipoles to follow the fast variation of the alternating applied electric field. Thus the dispersion occurring in the lower frequency regime is attributed to interfacial polarization since the electronic and atomic polarizations remain, by and large, unchanged at these frequencies [30]. Such kinds of similar results were observed for other systems of ferrites [31–33]. The decrease in dielectric constant with frequency can be explained on the basis of Koops' phenomenological theory [20], which considers the dielectric structure as an inhomogeneous medium of two layers of the Maxwell–Wagner type [34].

Also, according to Rabinkin et al. [35], the polarization in ferrites is through a mechanism similar to the conduction process. The presence of Fe^{3+} and Fe^{2+} ions render ferrite materials to be dipolar. Rotational displacement of dipoles results in orientational polarization. In ferrites, rotation of $Fe^{2+} \leftrightarrow Fe^{3+}$ dipoles may be visualized as the exchange of electrons between the ions so that the dipoles align themselves in response to the alternating field. The existence of inertia to the charge movement would cause relaxation of the polarization. The polarization at lower frequencies results from electron hopping between $Fe^{3+} \leftrightarrow Fe^{2+}$ ions in the ferrite lattice. The polarization decreases with increase in frequency and reaches a constant value due to the fact that beyond a certain frequency of external field the electron exchange $Fe^{3+} \leftrightarrow Fe^{2+}$ cannot follow the alternating field [36]. In the present study, it was observed that the dielectric constant increases with increasing calcination temperature. This may be due to the decrease in resistivity of cobalt ferrite with calcination temperature, as the dielectric constant is directly proportional to the square root of conductivity [37].

3.4.2.2. ac conductivity. In order to understand the conduction mechanism and the type of polarons responsible for conduction, the variation of ac conductivity as a function of frequency is represented in Fig. 7. It is also well known that, in large polaron hopping, the ac conductivity decreases with frequency whereas in small polaron hopping it increases with frequency [38,39]. The electrical conduction mechanism in terms of the electron and polaron hopping model has been discussed by Austin and Mott [40]. In the present case, the plots for ac conductivity measurement are linear, indicating that the conduction is due to small polarons. It has been shown that, for ionic solids, the concept of small polaron is valid [41]. As the frequency of the applied field increases, the conductive grains become more active, thereby promoting electron hopping between two adjacent octahedral sites (B-sites) in the spinel lattice and a transition between Fe^{2+} and Fe^{3+} ions, thereby increasing the hopping conduction. Therefore a gradual increase in conductivity was observed with frequency. As reported by Alder and Fienleib [42], the frequency-dependent conduction is mainly attributed to a small polaron-type hopping mechanism.

4. Conclusion

The nanocrystalline cobalt ferrite was successfully synthesized by employing combustion method using hexamethylenetetramine (hexamine) as a fuel for the first time. The TGA measurements show the stable phase formation takes place above 700 °C. The XRD study reveals the formation of cubic spinel structure with all the characteristic reflections having most intense (3 1 1) reflection. The particle size of cobalt ferrite increases with increasing calcination temperature. The resistivity of $CoFe_2O_4$ decreases with increasing calcination temperature. The dielectric constant increases with the calcination temperature and all the samples exhibit usual dielectric dispersion which is due to the Maxwell–Wagner-type interfacial polarization. The ac conductivity measurement suggests that the conduction is due to small polaron hopping.

Acknowledgements

One of the authors, R.C. Kambale is grateful to the Council of Scientific and Industrial Research (CSIR) of Human Resource Development Group, New Delhi, Government of India, for providing the financial support to carry out this research work. Also, the author, J.Y. Patil acknowledges DAE-BRNS for the grant of JRF. All the authors gratefully acknowledge DAE-BRNS, India for the financial support.

References

[1] D. Goll, H. Kronmuller, Naturwissenschaften 87 (2000) 423.
[2] M. Sugimoto, J. Am. Ceram. Soc. 82 (1999) 269.
[3] W.G. Wang, M. Mogensen, Solid State Ionics 176 (2005) 457.
[4] J. Prodelalova, B. Rittch, A. Spanova, K. Petrova, M.J. Beneg, J. Chromatogr. A 1056 (2004) 43.
[5] A. Spanova, B. Rittich, M.J. Benes, D. Horak, J. Chromatogr. A 1080 (2005) 93.

[6] T. Mathew, S. Malwadkar, S. Pai, N. Sharanappa, C. Sebastein, C.V.V. Satyanarayana, V.V. Bokade, Catal. Lett. 91 (2003) 217.
[7] S.A. Chambers, R.F.C. Farrow, S. Maat, M.F. Toney, L. Folks, J.G. Catalano, T.P. Trainor, G.E. Brown Jr., J. Magn. Magn. Mater. 246 (2002) 124.
[8] M.C. Terzzoli, S. Duhalde, S. Jacobo, L. Steren, C. Moina, J. Alloys Compd. 369 (2004) 209.
[9] T. Pannaparayil, S. Komarneni, IEEE Trans. Magn. 25 (1989) 4233.
[10] F. Congiu, G. Concas, G. Ennas, A. Falqui, D. Fiorani, G. Marongiu, S. Marras, G. Spano, A.M. Alberto, M. Testa, J. Magn. Magn. Mater. 272–276 (2004) 1561.
[11] C.H. Yan, Z.G. Xu, F.X. Cheng, Z.M. Wang, L.D. Sun, C.S. Liao, J.T. Jia, Solid State Commun. 111 (1999) 287.
[12] N. Moumen, P. Veillet, M.P. Pileni, J. Magn. Magn. Mater. 149 (1995) 67.
[13] M. Rajendran, R.C. Pullar, A.K. Bhattacharya, D. Das, S.N. Chintalapudi, C.K. Majumdar, J. Magn. Magn. Mater. 232 (2001) 71.
[14] L.J. Cote, A.S. Teja, A.P. Wilkinson, Z.J. Zhang, Fluid Phase Equilib. 210 (2003) 307.
[15] F.X. Cheng, Z.Y. Peng, C.S. Liao, Z.G. Xu, S. Gao, C.H. Yan, Solid State Commun. 107 (1996) 471.
[16] N. Hanh, O.K. Quy, N.P. Thuy, L.D. Tung, L. Spinu, Phys. B: Condens. Matter 327 (2003) 382.
[17] K.C. Patil, S.T. Aruna, S. Ekambaram, Curr. Opin. Solid State Mater. Sci. 2 (1997) 158.
[18] N. Blazevic, D. Kolbah, B. Belin, V. Sunjic, F. Kajfez, Synthesis 14 (1979) 161.
[19] A.D. Shaikh, V.L. Mathe, J. Mater. Sci. 43 (2008) 2018.
[20] C.G. Koops, Phys. Rev. 83 (1951) 121.
[21] R.C. Kambale, P.A. Shaikh, C.H. Bhosale, K.Y. Rajpure, Y.D. Kolekar, J. Smart Mater. Struct. 18 (2009) 115028.
[22] A.S. Prakash, A.M.A. Khadar, K.C. Patil, M.S. Hegde, J. Mater. Synth. Process. 10 (3) (2002) 135.
[23] S.R. Jain, K.C. Adiga, V.R. Pai Verneker, Combust. Flame 40 (1981) 71.
[24] R.D. Waldron, Phys. Rev. 99 (1955) 1727.
[25] R.S. Devan, Y.D. Kolekar, B.K. Chougule, J. Phys.: Condens. Matter 18 (2006) 9809.
[26] E.J.W. Verwey, J.H. De Boer, Rec. Trav. Chim. Pays-B. 55 (1936) 531; R. Parker, H. Lords, R. Phys. Soc. 79 (1962) 383.
[27] G. Dietzmann, M. Krotzch, S. Wolf, Phys. Stat. Sol. 2 (1962) 1762.
[28] B. Vishwanathan, V.R.K. Murthy, Ferrite Materials Science and Technology, Narosa Publ. House, New Delhi, 1990.
[29] R.C. Kambale, P.A. Shaikh, C.H. Bhosale, K.Y. Rajpure, Y.D. Kolekar, Smart Mater. Struct. 18 (2009) 085014.
[30] E. Veena Gopalan, K.A. Malini, S. Saravanan, D. Sakthi Kumar, Y. Yoshida, M.R. Anantharaman, J. Phys. D: Appl. Phys. 41 (2008) 185005.
[31] M.A. Ahamed, M.A. Elhiti, J. Phys. III 5 (1995) 775.
[32] A.M. Shaikh, S.S. Bellard, B.K. Chougule, J. Magn. Magn. Mater. 195 (1999) 384.
[33] M.A. Ahamed, M.A. Elhiti, E.I. Nimar, M.A. Amar, J. Magn. Magn. Mater. 152 (1996) 391.
[34] K.W. Wagner, Am. Phys. 40 (1973) 317.
[35] L.T. Rabinkin, Z.I. Novikova, Ferrites, Minsk: Acad. Nauk. USSR, 1960, p. 146.
[36] N. Popandian, P. Balay, A. Narayanasamy, J. Phys.: Condens. Matter 14 (2002) 3221.
[37] M. George, S.S. Nair, K.A. Malini, P.A. Joy, M.R. Anantharaman, J. Phys. D: Appl. Phys. 40 (2007) 1593.
[38] R.S. Devan, B.K. Chougule, J. Appl. Phys. 101 (2007) 014109.
[39] R.P. Mahajan, K.K. Patankar, M.B. Kothale, S.A. Patil, Bull. Mater. Sci. 23 (2000) 273.
[40] I.G. Austin, N.F. Mott, Adv. Phys. 18 (1996) 411.
[41] K.K. Patankar, S.S. Joshi, B.K. Chougule, Phys. Lett. A 346 (2005) 337.
[42] D. Alder, J. Fienleib, Phys. Rev. B 2 (1970) 3112.